Journal of Applied Electrochemistry (2005) 35:487–498
DOI 10.1007/s10800-004-8343-5

Determination of heterogeneities in a scraped surface heat exchanger using electrochemical sensors

FRANCINE FAYOLLE[1,*], JÉRÔME MABIT[1] and JACK LEGRAND[2]
[1]*Département Génie des Procédés Alimentaires, GEPEA – UMR 6144 CNRS, Ecole Nationale d'Ingénieurs des Techniques des Industries Agricoles et Alimentaires, Rue de la Géraudière – BP 82225, 44322 Nantes Cedex 3, France*
[2]*GEPEA – UMR 6144, CNRS, Université de Nantes CRTT, BP 406, 44602 Saint Nazaire Cedex, France*
*(*author for correspondence: phone +33-2-51-78-54-80; fax +33-2-51-78-54-67; e-mail: fayolle@enitiaa-nantes.fr)*

Received 05 June 2004; accepted in revised form 15 December 2004

Key words: electrochemical technique, flow visualisation, scraped surface heat exchanger, shear heterogeneities, spiral flow, wall shear rates

Abstract

An experimental investigation of a scaled-down model of an industrial exchanger, using an electrochemical technique, was undertaken in order to show the presence of hydrodynamic heterogeneities at low axial Reynolds number. Heterogeneities were revealed in the bowls with respect to the generalised Taylor number as the result of the perturbations added to the flow by blade rotation at both ends of the exchanger. Shear heterogeneities associated to flow visualisations were correlated to temperature heterogeneities observed in the bowls. Shear fluctuations were revealed in the scraped part describing two distinctive zones at low rotation speed caused by varying viscosity in the flow field. A complex spiral flow was observed by flow visualisation characterising a mass transfer evolution comprised between these two distinctive zones at low Taylor number.

Nomenclature

C_0	bulk concentration (mol m^{-3})	$Re_r = \frac{\rho N d_r^2}{\eta}$	Rotational Reynolds number (–)
D	diffusion coefficient (m^2 s^{-1})	R_r	rotor radius (m)
d	diameter of the microelectrode (m)	R_s	stator radius (m)
d_h	hydraulic diameter (m) $d_h = (d_s–d_r)$	S	wall shear rate (s^{-1})
		Sc	exchange surface (m^2)
d_r	rotor diameter (m)	T	temperature (°C)
d_s	stator diameter (m)	$Ta = \sqrt{\frac{R_s-R_r}{R_r}}\frac{\rho d_h}{2}\frac{(\Omega R_r)}{\eta}$	Taylor number (–)
e	gap (m)	$Ta_g = \sqrt{\frac{R_s-R_r}{R_r}}\frac{\rho d_h^n}{2^n}\frac{(\Omega R_r)^{2-n}}{K}$	generalised Taylor number (–)
F	Faraday constant (A s mol^{-1})	Ta_c, Ta_{gc}	critical values of Taylor number (–)
K	consistency coefficient of the product (Ostwald law (Pa s^n))	U_d	mean axial velocity in the annular space (m s^{-1})
L	stator length (m)	z	number of electrons (–)
n	flow behaviour index of the product (Ostwald law (–))	ρ	density (kg m^{-3})
		η	dynamic viscosity (Pa s)
N	rotation speed (rps)	γ	shear rate (s^{-1})
n_L	number of blades (–)	Ω	rotating speed of the rotor (rad. s^{-1}); $\Omega = 2\pi N$
Q	flow rate (m^3 s^{-1})		
$Re_{ax} = \frac{\rho U_d d_h}{\eta}$	axial Reynolds number (–)	τ	shear stress (Pa)
$Re_{axg} = \frac{\rho U_d^{2-n} d_d^n}{K}$	generalised axial Reynolds number (–)		

1. Introduction

In the food and chemical industries, scraped surface heat exchangers are widely used for heating or cooling viscous fluids. Blades mounted on a rotating shaft continuously remove the product in contact with the exchange surface, at the same time inducing radial mixing and increasing the heat transfer rate. In this type

of apparatus, the flow is the result of the superposition of annular Poiseuille flow and Taylor–Couette flow, on which perturbations are added by blade rotation. The presence of Taylor vortices was observed when the dimensionless number reached a critical value ($Ta_{gc} \simeq 80$, Dumont et al. [1]). Investigations in the area of scraped surface heat exchangers have been primarily concerned with the experimental determination of thermal performance. The influence of the flow rate, rotation speed, number of blades and gap width have been studied as well as the viscosity and other properties of the fluid [2–5].

Hydrodynamic behaviour has also been studied to propose shear stress prediction models [6–9] and to determine the transition from laminar to vortex flow [1, 7, 8]. A few studies have reported the presence of thermal or hydrodynamic heterogeneities. Maingonnat et al. [7] have shown different thermal and hydrodynamic behaviour for Taylor numbers less than 100. Maingonnat and Corrieu [3] reported that axial heat diffusion considerably influenced temperature homogeneities at the inlet of the exchanger. Dumont et al. [10] confirmed these observations with thermal measurements in bowls at low Taylor number ($Ta_g < 10$). From the hydrodynamic point of view, experimental and numerical studies have been realised and the presence of vortices has been identified, in particular Taylor vortices which were visualised by Naimi [8] and Dumont et al. [1] for Ta_g values from 61 to 80, depending on product properties. Taylor vortices appear at the outlet and move throughout the exchanger towards the inlet bowl. Dumont et al. [1] have visually distinguished three different zones along the exchanger and demonstrated that vortices are thwarted by blades in rotation. They have shown, using an electrochemical method, the presence of high wall shear rates at the scraped exchange surface. Blade scraping caused high perturbations at the surface and a large increase in shear stress was observed. De Goede and De Jong [11] numerically predicted the development of a vortex between the scraper blades and Baccar and Abid [12] predicted two stagnant zones, one in the neighbourhood of the rotor and the second located at the rear side of the scraper ($Re_r = 90$, $Re_{ax} = 3$). Stranzinger et al. [13] improved numerical studies using a finite volume method applied to Newtonian and inelastic non-Newtonian fluids ($n = 0.65$). They showed that closed streamline loops or vortices are formed between the blades and that a secondary flow exchange takes place between the leading and the trailing edges of the blades along the outer cylinder wall. All numerical studies reveal the appearance of heterogeneities for specific conditions of Taylor number leading to heterogeneous thermal treatment.

The aim of this work is to investigate heterogeneities by means of an electrochemical technique in all zones of the exchanger in flow conditions prior to vortex appearance, as well as in vortex flow. The motivation was to analyse the distribution of shear stresses and how the mechanical energy was dissipated in a scraped surface heat exchanger. Average energy dissipation often does not make physical sense for food products, in particular for highly sensitive products. The determination of the different levels of mechanical treatment is important for food processing. Moreover, the relationship between energy distribution and flow regime is also very significant in process control.

The evolution of the limiting diffusion current and the wall shear rates obtained with microelectrodes are analysed for Newtonian and non-Newtonian highly viscous products. Heterogeneities revealed are presented and discussed with respect to generalised Taylor number and compared with results obtained by visualisation experiments.

2. Materials and methods

2.1. *Scaled-down model of SSHE*

The work was carried out on a scaled-down model of an industrial exchanger (Duprat TR 13×60). All dimensions are given previously [14, 15]. The scaled-down model was used to measure shear stress and understand hydrodynamic behaviour. This model was built in order to present the same thermal behaviour as that obtained in the industrial SSHE, with variations of thermal heterogeneities [16]. The design principle was to keep the same order of magnitude of Ta_g obtained in the industrial exchanger ($0 < Ta_g < 100$).

The pilot plant included an inlet tank, a pump, the model heat exchanger, an electromagnetic flow meter, (Promag, Endress + Hausser), an optical fibre detection system of blade presence and an experimental apparatus for the electrochemical technique.

2.2. *Electrochemical technique*

Measurement of wall shear rates at the surface of different elements of the SSHE was carried out using circular platinum microelectrodes with a diameter, d of about 0.4 mm (calibrated precisely afterward). Sixteen microelectrodes were fixed as shown on Figure 1: four on the rotor (no. 1, 2, 3, 4), three on the leading edge of the blades (no. 6, 8, 10), three on the rear face (no. 5, 7, 9) and three at the surface of each bowl (inlet: no. 11, 12, 13; outlet: no. 14, 15, 16). All microelectrodes had a circular shape, except those embedded into the walls of the bowls. The bowl microelectrode shape was not circular but oval. Reiss and Hanratty [17] have determined for a circular microelectrode that the wall shear rate, S can be related to the limiting diffusion current, I (Eq. (1)):

$$S = \left(\frac{1.447}{zF}\right)^3 \frac{I^3}{D^2 C_0^3 d^5}, \tag{1}$$

where z is the number of electrons involved in the redox reaction, F the Faraday constant, d the diameter of the

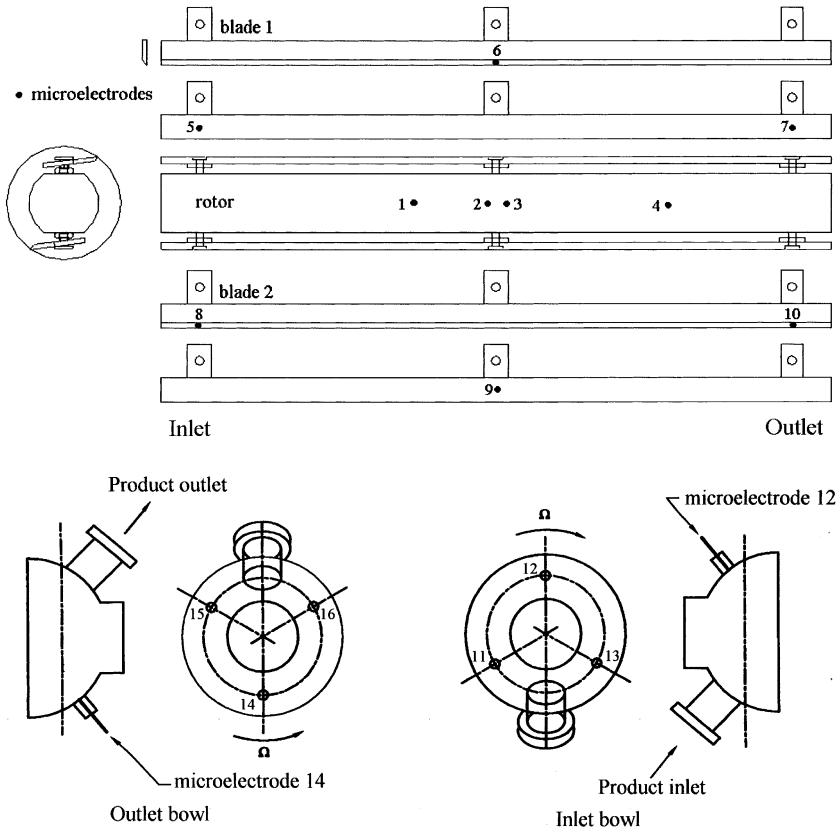

Fig. 1. Schematic representation of microelectrodes on the stator, the rotor, bowl and the blades of the SSHE.

circular microelectrode, C_0 the bulk concentration of the active ions and D the diffusion coefficient of these ions in solution.

The non-circular shape leads to a small error with respect to Eq. (1). However, there is only a 6% difference in the numerical constant between circular and rectangular microelectrodes [17], and no significant difference is observed between the surface area of microelectrodes inserted in the bowl or in the blades. Despite the oval shape, these microelectrodes were considered circular and Eq. (1) was used to analyse experimental data.

The stainless-steel shaft served as an auxiliary electrode in the electrochemical cell and the well-known ferri–ferrocyanide ionic system ($Fe(CN_6)^{3-} + e^- \leftrightarrow \ddagger Fe(CN_6)^{4-}$) was used with a large excess of supporting electrolyte (K_2SO_4)to eliminate migration phenomena. Microelectrodes embedded in the rotor were isolated with epoxy. A transient technique developed by Sobolík et al. [18] was reproduced to accurately measure the actual surface area of the microelectrode.

2.3. *Characteristics of the electrolytes*

Two polymeric solutions were used: a Newtonian and a shear-thinning fluid. The viscosity measurements were performed at 25 °C with a Couette rheometer TA Instrument AR 1000 with imposed torque.

Emkarox HV 45 is a mixture of polypropylene glycol and polyethylene glycol. In this work, an Emkarox HV45 solution (44% w/w of water), from ICI, was used. The dynamic viscosity of the Emkarox HV45 solution was 3.7 Pa s at 25 °C. Different proportions were added to water and electrolyte to obtain different viscosities. The electrolyte consisted of a mixture of potassium ferricyanide, potassium ferrocyanide and potassium sulphate as supporting electrolyte. The viscosities of the different aqueous solutions are given in Table 1.

Aqueous solutions of carboxymethylcellulose (CMC, high viscosity from Sigma) have a pseudoplastic behaviour, the non-Newtonian characteristics depending on the CMC concentration. CMC powder was progressively added to agitated cold water. After dissolution of CMC sodium salt, potassium sulphate and potassium ferricyanide and ferrocyanide were added to the electrolyte. The rheological behaviour was modelled by two different power-laws according to the shear rate domains applied in the rheometer: 5–80 s^{-1} and 50–1230 s^{-1}. The physical properties of CMC electrolyte are summarised in Table 1. The determination of the diffusion coefficients of the ferricyanide ions, D, in these polymeric solutions is described in Legrand et al. [19].

2.4. *Operating conditions*

Wall shear rates were measured in isothermal conditions ($T = 25°C$) at low axial Reynolds number. Operating conditions were: flow rate ($Q = 0$, 35 and 100 l h^{-1}), rotation speed of the rotor (N varied from 1 to 10 rps) and product temperature ($T = 25°C$). Data acquisitions

Table 1. Physical properties of Emkarox HV45 and CMC solutions at 25 °C

Solution	Water w/w	ρ/kg m^{-3}	$K_3[Fe(CN)_6]$ /mol m^{-3}	$K_4[Fe(CN)_6]$ /mol m^{-3}	K_2SO_4 /mol m^{-3}	$10^{10}D$/ m^2 s^{-1}	η/ Pa s	n	K/ Pa s^n	n	K/Pa s^n
HV45–75%	25%	1079	5.304	5.304	127.3	0.70	0.84				
HV45–60%	40%	1071	5.241	5.241	209.6	1.15	0.32				
Solution/weight%											
CMC 0.5%		1046	5.0	5.0	300	7.50		0.85	0.11	0.73	0.16
CMC 0.7%		1071	5.0	5.0	500	7.50		0.78	0.36	0.65	0.63
CMC 1.0%		1047	4.0	4.0	300	7.50		0.66	1.64	0.51	3.02
								Shear rate domain $\dot{\gamma}$/s^{-1}			
								5–80		50–1234	

of the limiting current were carried out with a numerical recorder (Digital Audio Tape Tekelec RD-145T with 16 channels), which allowed simultaneous recordings of diffusion current on different microelectrodes. The sampling frequency of the recording was 6000 Hz. For each rotation speed, N, the limiting diffusion currents from the microelectrodes were numerically recorded over 60 s. A rotary collector (Litton EC3848) ensured the signal continuity between microelectrodes in rotation (rotor and blades) and the data acquisition system.

3. Results and discussion

The time-fluctuations of the limiting diffusion current are observed on microelectrodes fixed on the rotor (Figure 2) and the blades (Figure 3) at low rotation speed ($N = 2$ rps). The period of the fluctuations corresponds to one rotation of the rotor and their amplitude is more significant on the rear face of blades (microelectrode no. 7) than on the rotor and the leading edge (microelectrode no. 10). At $N = 1$ rps, the time-evolution of the limiting diffusion current on the rotor shows that the signal is nearly constant with a minimum observed at each rotation. This constant evolution of the signal between two minima tends to disappear with increasing rotation speed; a periodic evolution is finally observed for the limiting current ($N = 2$ rps; Figure 3). These heterogeneities remain with large increase in rotation speed but their intensity decreases, as shown in Figure 4. For CMC solution at 0.7%, the transition from laminar to vortex flow is obtained for a critical value of Taylor

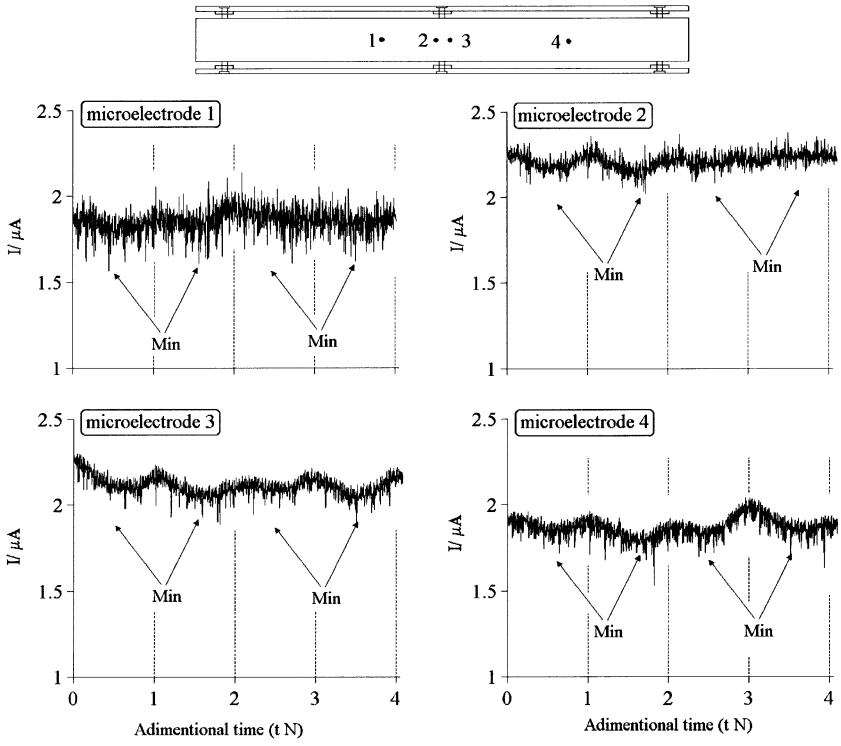

Fig. 2. Variation of limiting diffusion current on the rotor with respect to number of blade rotations for CMC 0.7%; ($Q = 35$ l h^{-1}; $N = 2$ rps; $Re_{axg} = 0.1$; $Ta_g = 12.1$).

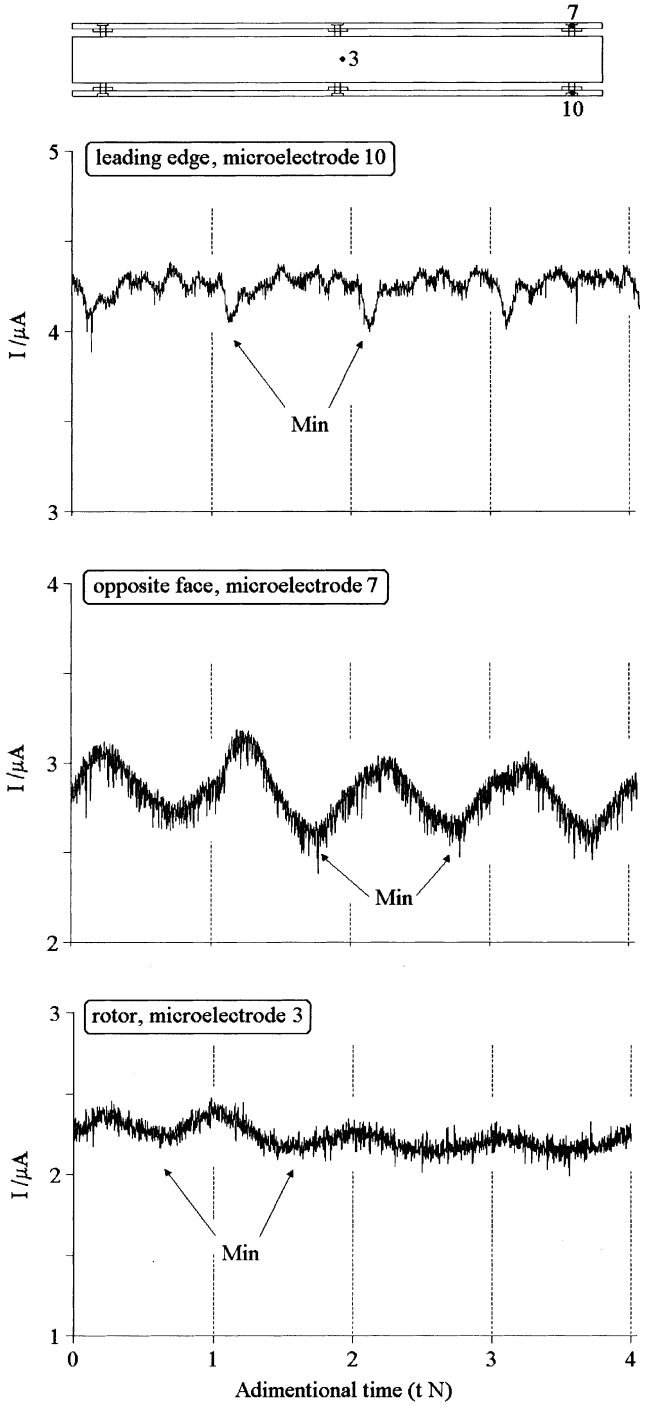

Fig. 3. Variation of limiting diffusion current on blades and rotor with respect to number of blade rotations for CMC 0.7%; ($Q = 35\ l\ h^{-1}$; $N = 2$ rps; $Re_{axg} = 0.1$; $Ta_g = 12.1$).

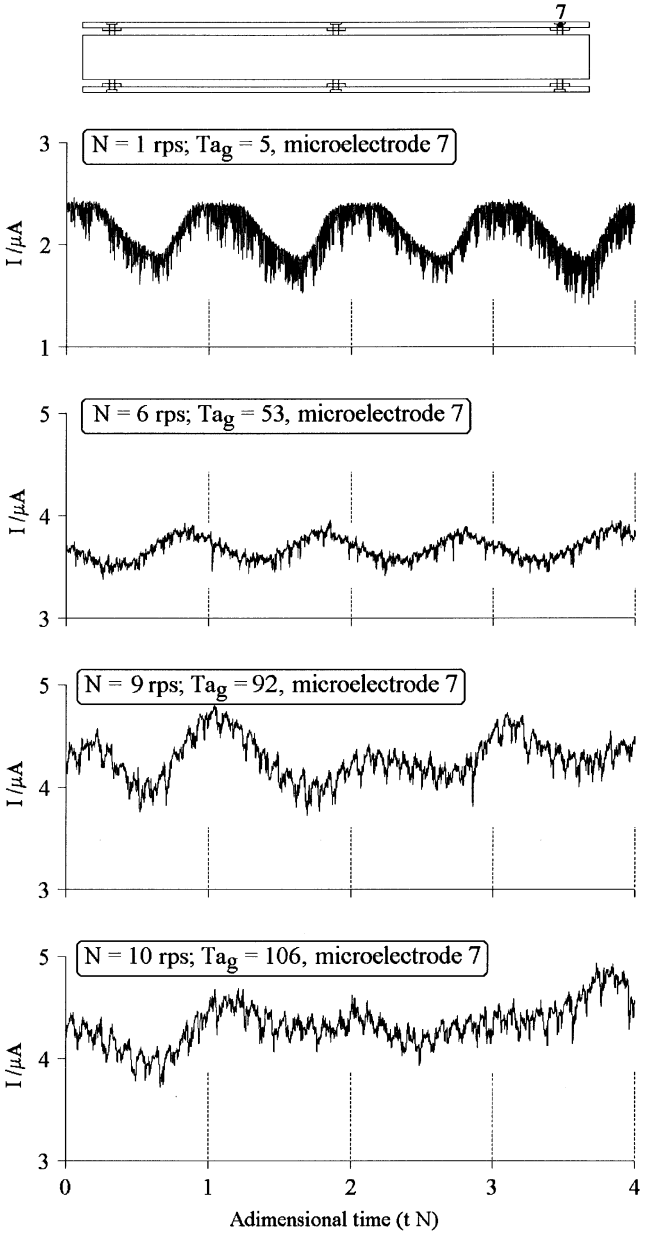

Fig. 4. Variation of limiting diffusion current on the rear side of the blade with respect to number of blade rotations for CMC 0.7%; ($Q = 35\ l\ h^{-1}$).

number of $Ta_{gc} \asymp 80$. The presence of Taylor vortices for $Ta_g > 80$ perturbs the periodic-evolution of the diffusion current.

On the rotor, the intensity of the signal is higher close to a fixing point which indicates greater shear rates. Microelectrodes were mounted on a generatrix of the cylinder, as shown in Figure 1, leading to a synchronisation of the time-evolution of the diffusion current recorded on these microelectrodes (Figure 2). In contrast, a time shift occurs between different signals observed on the rotor, the leading edge and the rear face of the blades (Figure 3). As shown in Figure 1, microelectrodes were not positioned on the same radial axis. The time-evolution of the diffusion current and the signal given by the optical fibre for the detection of blade passage allows association of the evolution of the diffusion current given by each microelectrode to the blade passage [15]. In our case, blade no. 1 is the reference blade for the signal given by the fibre optic system. The minimum limiting diffusion current is always observed when the microelectrode passes through a specific zone in the SSHE. Similarly, the maximum current is located in an equivalent zone opposite to the zone with the minimum current (Figure 5). At the same axial position of the SSHE,

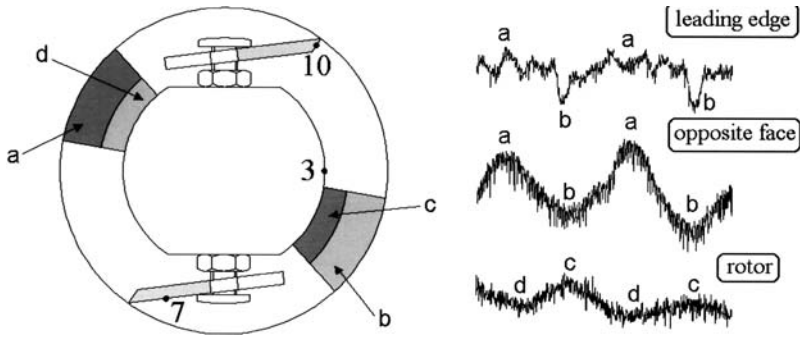

Fig. 5. Schematic representation of shear heterogeneities in the cylinder of the SSHE; ($Q = 35\ l\ h^{-1}$; N = 2 rps, $Re_{axg} = 0.1$; $Ta_g = 12.1$).

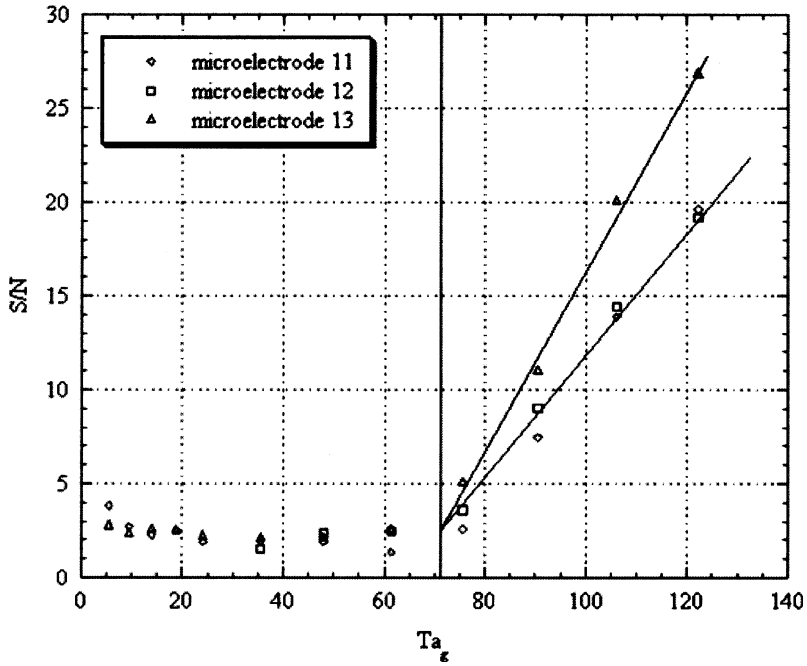

Fig. 6. Evolution of S/N in the inlet bowl (CMC 0.7%; $Q = 35\ l\ h^{-1}$).

the maximum current measured on the rotor is in front of the minimum measured at the leading edge and the rear face of the blades. Inversely, on the other side of the exchanger, the minimum current observed at the rotor is in phase with the maximum observed on the blades. In fact, two zones with high shear perturbations are visualised (Figure 5). Furthermore, these fluctuations were also observed with no axial flow rate but with a lower intensity.

The study was extended to the inlet and the outlet bowl to identify the presence of heterogeneities. Each bowl was equipped with three microelectrodes mounted at 120°, as shown in Figure 1. The geometry of the bowls can be assimilated to annular spaces, in spite of an increase in volume due to the reduction in the rotor diameter. Unlike in the cylindrical part of the SSHE, no periodic variation is observed on the limiting diffusion current obtained with microelectrodes embedded into the walls of bowls. Figures 6 and 7 present the variation of the dimensionless ratio S/N in the inlet and the outlet bowl of the exchanger. S/N values are relatively low and constant for $Ta_g < 66$–72 and the regime is considered laminar. For $Ta_g > 66$–72, a significant increase in S/N is observed due to the appearance of Taylor vortices. They appear for $Ta_g > 45$ in a classical annular space [20] and for $Ta_g > 80$ with blades [1]. For $Ta_g > 100$, S/N values are higher at the bottom of the bowl measured by microelectrode no. 14 (Figure 7). This zone of the bowl is located opposite to the product outlet pipe, where the product deviates from axial flow to leave the exchanger. In the same way, at the inlet, microelectrode no. 13 mounted in the bottom part of the bowl shows S/N values higher than in the rest of the bowl. An increase in flow rate from 35 to 100 $l\ h^{-1}$ (Re_{axg} from 0.63 to 2.38) does not reveal a high increase in shear; S/N values are similar (Figure 8). At low axial Reynolds number, flow behaviour is mainly controlled by the rotational flow and the presence of Taylor vortices.

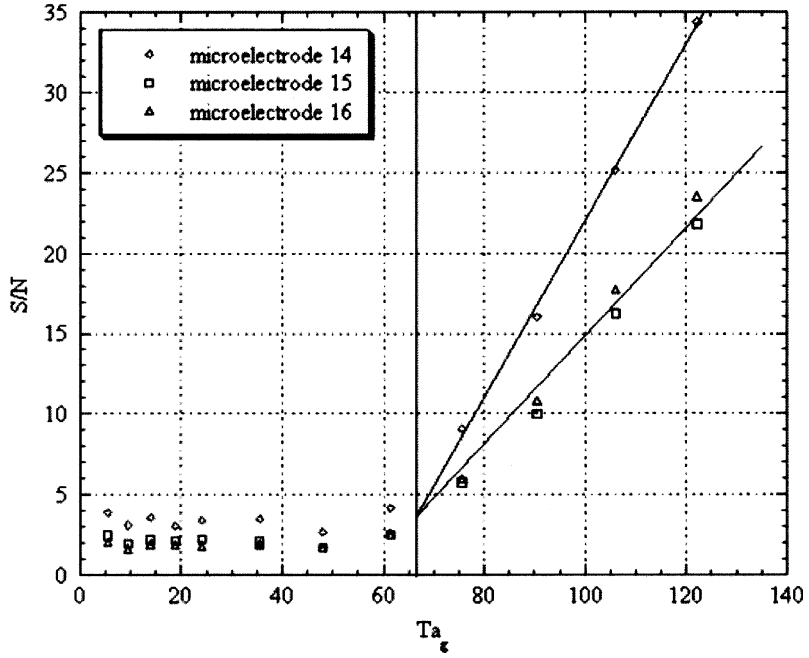

Fig. 7. Evolution of S/N in the outlet bowl (CMC 0.7%; $Q = 35\ \mathrm{l\ h^{-1}}$).

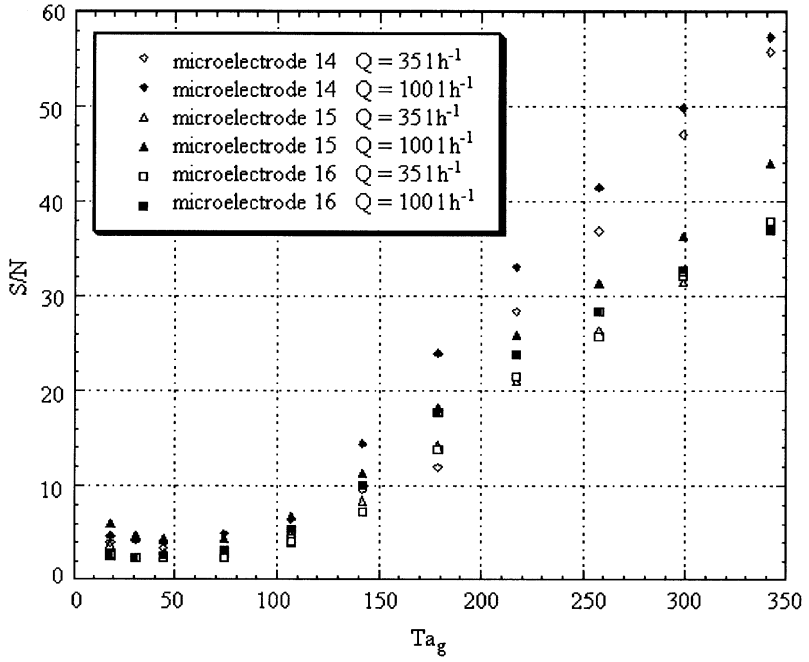

Fig. 8. Evolution of S/N in the outlet bowl for CMC 0.5%.

As pointed out before, increase in S/N is related to vortex flow. The shape and flow of Taylor vortices in the outlet bowl can be deduced from the time-evolution of the current for microelectrodes no. 15 and 16 for $\mathrm{Ta_g} = 107$ and $Q = 35\ \mathrm{l\ h^{-1}}$ (Figure 9). The limiting diffusion current shows periodic variation of current, the minimum corresponds to the inflow boundary while the maximum corresponds to the outflow boundary. At the bottom of the outlet bowl, the current variation given by microelectrode no. 14 clearly does not show this periodicity; the evolution is disturbed and deformation of vortices cannot be excluded. In the inlet bowl, the presence of vortex cells is not clearly identified by the time-variation of the current.

3.1. *Periodic fluctuation of limiting diffusion current in the scraped part*

Fluctuations observed in the cylindrical part have a periodicity of one rotation as demonstrated previously (Figures 2 and 3). These perturbations can be the result of a flow singularity at each rotation of the rotor. The

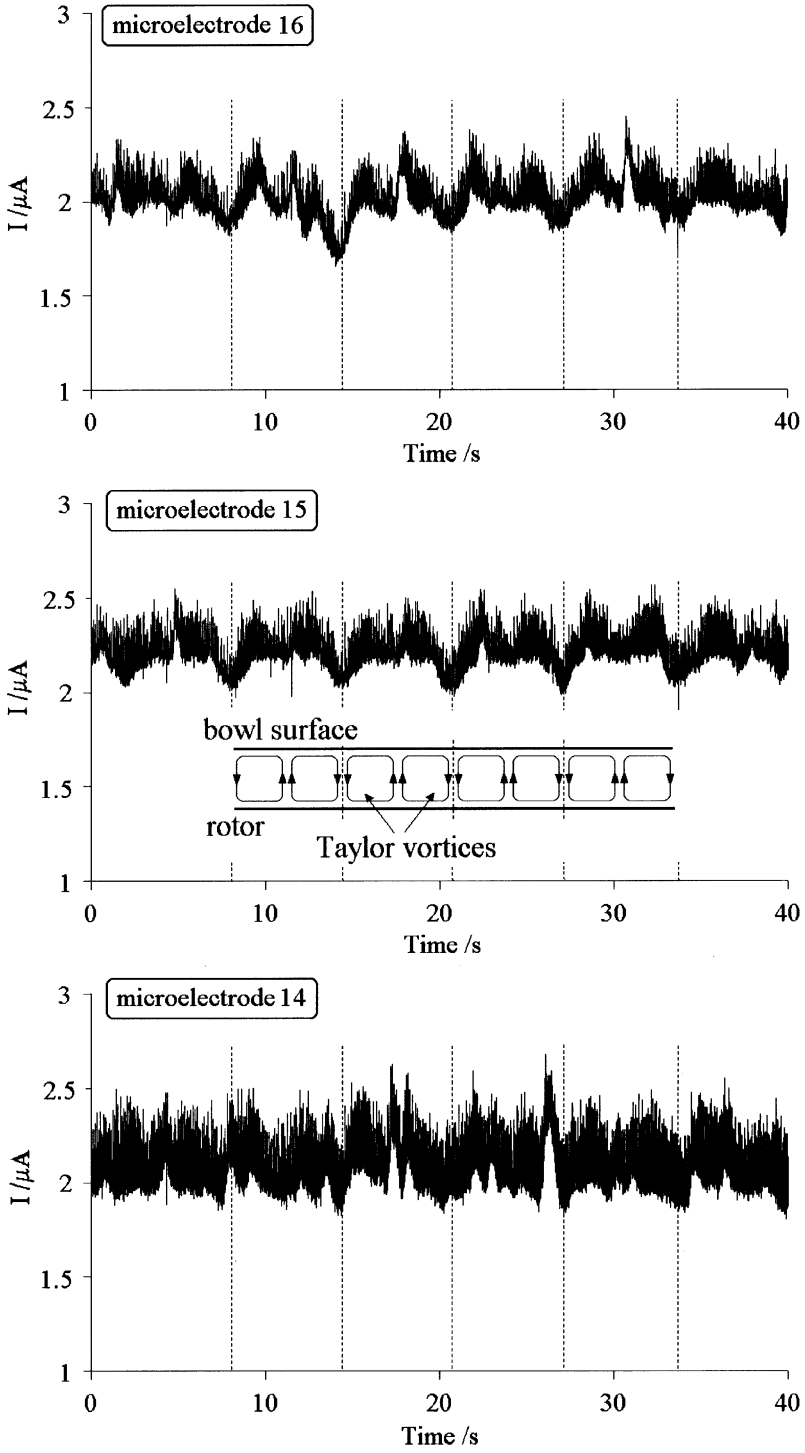

Fig. 9. Time evolution of limiting diffusion current for CMC 0.5% in outlet bowl SSHE ($Q = 35\ l\ h^{-1}$; $N = 4$ rps; $Ta_g = 107$; $Re_{axg} = 0.63$).

influence of the blades and the rotor can be excluded because of the rotation of these elements. Only bowls and the outer wall surface are kept fixed. Rotation of the stator with an angle of 90° does not change the position of the fluctuations. Thus, the fluctuations cannot be due to non-symmetry of the outer cylinder. Only bowls located at both ends of the exchanger show fixed singularities which may be responsible for the fluctuation. The bowls are similar but mounted in opposition on a vertical axis; inlet and outlet are located at the bottom and top of the exchanger, respectively (Figure 1). However, the fluctuation of one rotation observed on the blades and the rotor was not identified on bowl microelectrodes. Thus, the periodic fluctuation is not due to the non-symmetric fluid inlet in the bowl.

Flow visualisations were made using a stator made of transparent Altuglass with a Newtonian solution of Emkarox HV45 with 40% w/w of water and a non-Newtonian solution of CMC at 0.7% w/w in order to achieve the same order of low Ta_g at low

rotation speed and to explain the origin of these periodic fluctuations prior to the appearance of vortex flow. The marker used in this case was bettanin (concentrated red beet juice) injected at the top of the inlet bowl. Image capture was realised with a numerical video camera (Sony TRV 900) on top of the stator in order to visualise the two distinctive zones showing high shear fluctuations. The capture frequency was 25 images per second. The video analysis shows that a spiral was developed on the rotor for 0.7% w/w CMC solution and for $Ta_g = 8$. A sketch of bettanin flow behaviour is shown on Figure 10. The trajectories were increasingly shorter as the rotation speed increased; the space between the spirals was increasingly reduced. The spiral flow explains why the maximum of shear fluctuation is located on one side at the rotor and on the other side at the outer wall surface, as shown in Figure 5. The development of spiral flow is often cited in this geometry for a low axial Reynolds Number. Härröd [4] indicated that Taylor vortices are created from a spiral at low axial flow. Balasubramaniam and Sastry [21] specified that the flow field in a SSHE is a complex function of axial and rotational component velocities, resulting in a spiral flow pattern; at low rotation speeds ($N \leq 2$ rps), elongated spiral trajectories were observed on the rotor. Wronski and Jastrzebski [22] indicated that spiral flows of pseudoplastic liquids are characterised by variability of viscosity in the flow field. Nouar [23] indicated that the heating of the outer wall surface had a destabilising effect on the vortices in an annular space leading to a spiral form, a radial gradient of temperature caused a radial gradient of viscosity, as well as a radial gradient of density. In a scraped surface heat exchanger used for shear-thinning fluids (CMC solutions in our case), the high level of shear encountered at the wall scraped surface reduces the apparent viscosity. The development of a spiral on the rotor was not observed for the Newtonian Emkarox solution, only elongated flow was visualised at the outer wall surface. This confirms that the presence of a spiral is due to the radial gradient of viscosity created by the radial gradient of shear rate promoted by blade rotation. Video recordings show that a small part of the product is flowing rapidly from spiral to spiral, with a velocity up to 17 times the flow velocity. This fluid flows because of a viscosity difference close to the stator surface. Indeed, as shown in Figure 5, a cross section of the flow can be represented by two concentric layers, the outer one located close to the exchange surface and covered by the path of rotating blades, the inner one near the rotor, submitted to hydrodynamic conditions. Near the rotor, mixing is only the result of the flow regime, while near the exchange surface, mixing is predominantly influenced by blade rotation. This difference in mixing conditions contributes to the production of shear heterogeneities in the radial direction, particu-

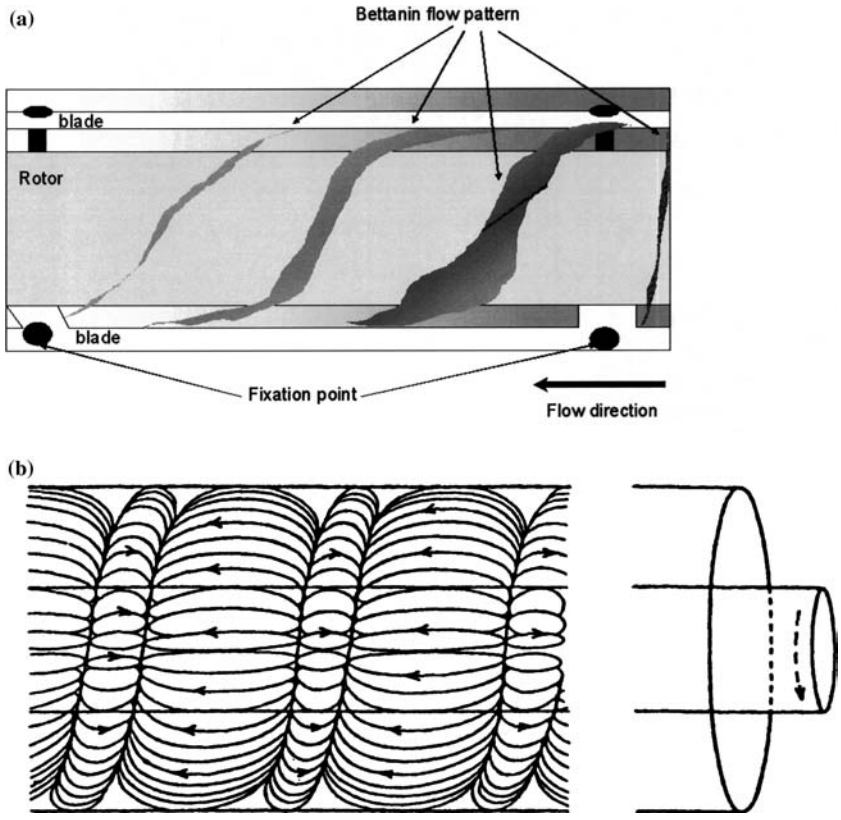

Fig. 10. (a) Spiral flow with a 0.7% w/w CMC solution ($Q = 35\ l\ h^{-1}$; $N = 1$ rps; $T = 25$ °C; $Ta_g = 8$; $Re_{axg} = 0.14$) (b) Helical structure of flow between two concentric cylinders (from Nouar [23])

larly at low rotation speed with a non-Newtonian fluid such as CMC. CMC viscosity decreases with increasing shear rates. However, blades are fixed on the rotor by three screws (Figures 1 and 5). The presence of these fixation points in the fluid inner layer (close to the rotor) creates new perturbations, which promotes mixing of the different zones. Some numerical studies [11, 24] show that vortices or secondary flow take place in the cylindrical part of the SSHE. Here, the presence of this particular flow is not clearly identified, but hydrodynamic heterogeneities are the result of complex flow influenced by blade design.

3.2. *Heterogeneities in bowls*

Dumont et al. [10] have carried out a thermal study in an industrial exchanger. The presence of thermal heterogeneities are noticed in bowls, at both inlet and outlet, for $Ta_g < 13.3$. Complete homogenisation is obtained for $Ta_g > 37$. The authors explain the appearance and evolution of these heterogeneities by the poor mixing action of the blades. This observation was previously made by Maingonnat et al. [7]; they indicated that thermal performance is independent of rotation speed for $Ta_g < 15$. Considering only the poor mixing efficiency of blades is not sufficient: heterogeneities found at the outlet are the result of many different events occurring in the whole exchanger. It is shown that the thermal treatment along the exchanger axis cannot erase heterogeneities observed in the inlet bowl. At low Taylor number ($Ta_g = 15$) and low rotation rate ($N = 2$ rps), flow visualisation shows that the fluid flowing out from the inlet bowl is stopped by the blade tip as well as by the first fixing screw. In the volume swept by the screw, the presence of the coloured tracer is much reduced. Thermal heterogeneities observed in the bowls are due to poor axial mixing as a result of the obstruction created by the fixing screw rotation. The residence time in a part of the inlet bowl corresponding to a dead zone is longer. Under these conditions, the product receives heterogeneous heat treatment in the inlet bowl itself, and heterogeneities persist up to the outlet.

For low Taylor numbers (below 60), hence before vortex generation, the dimensionless ratio S/N at both ends of the exchanger is different from one microelectrode to another. Although the ratio S/N remains lower than 5 (Figures 6 and 7), differences from 25 to 50% between microelectrodes are observed, indicating the presence of a heterogeneous flow.

In order to correlate heat transfer and flow heterogeneities, S/N evolution with respect to Ta_g in bowls were compared with results obtained by Dumont et al. [10] (Figures 11 and 12). These authors had measured temperature heterogeneities inside bowls, for different

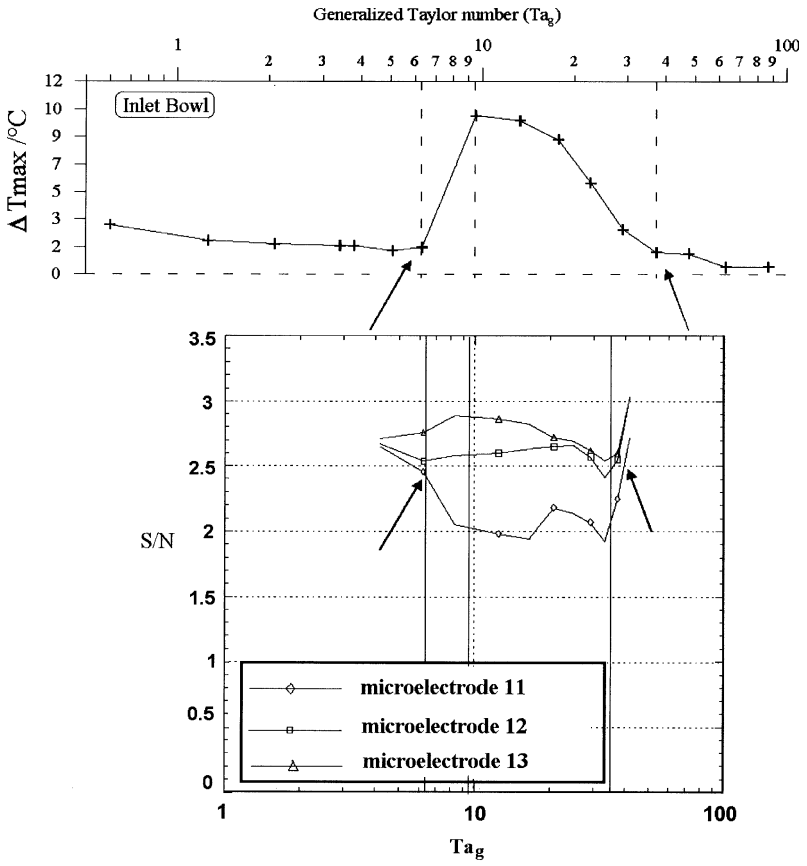

Fig. 11. Comparison between experimental S/N values obtained in inlet bowl for HV45–60% and thermal behaviour obtained by Dumont et al. [10].

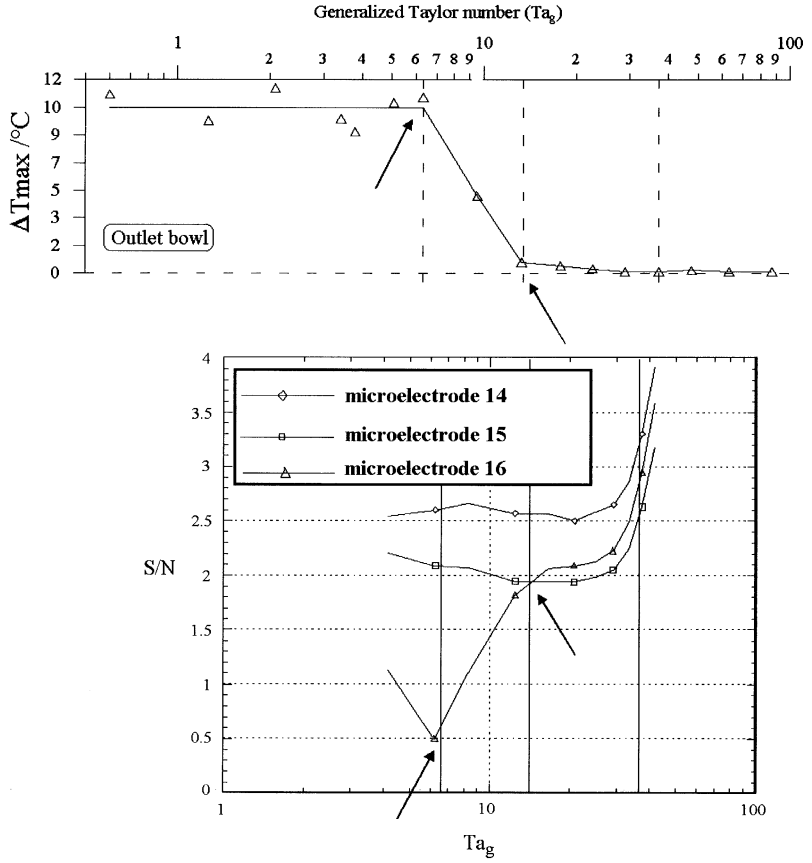

Fig. 12. Comparison between experimental S/N values obtained in outlet bowl for HV45–60% and thermal behaviour obtained by Dumont et al. [10].

values of Ta_g. Critical Taylor number values corresponding to a change in heat transfer regime presented by Dumont et al. [10] are reported on S/N values obtained in this work:

- At the inlet, heterogeneities observed on S/N values for $6.4 < Ta_g < 37$ correspond to the development of thermal heterogeneities. For critical Taylor numbers $Ta_g = 6.4$ and $Ta_g = 37$, S/N values are equivalent for all microelectrodes, and temperature is also homogeneous in the entire bowl.
- At the outlet, significant temperature heterogeneity was found by Dumont et al. [10] for $Ta_g < 6.4$ and high differences in shear rates were identified in the upper part. The thermal homogenisation observed when Taylor number increases, goes with a decrease in shear heterogeneities. On microelectrode no. 14 fixed in the bottom of the bowl, the S/N value is higher than in the rest of the bowl due to a change in the product flow direction in order to leave the SSHE through the top outlet as shown before.

Thus, thermal heterogeneities observed at low Taylor number in the laminar regime are correlated to shear heterogeneities measured at the wall surface of bowls. These heterogeneities result from the inefficiency of the blades to ensure good radial mixing at both ends of the exchanger at low rotation speed. According to our results and those of Dumont et al. [10], sufficient mixing is obtained in bowls by the development of a vortex flow for $Ta_g > 60$–70 which is an intermediate critical value in between that obtained for an annular space ($Ta_{gc} > 45$) and that obtained for a SSHE ($Ta_{gc} = 80$). The efficiency of thermal treatment remains questionable at low Ta_g promoting heterogeneous treatment quality.

4. Conclusion

An electrochemical method was used in a scaled-down model of an industrial exchanger to analyse hydrodynamic fluctuations with respect to Ta_g. The flow perturbations produced by blade rotation leads to a complex flow with shear heterogeneities developed all along the cylindrical part scraped by blades, particularly at low Taylor number. For non-Newtonian fluids, these shear heterogeneities lead to viscosity differences. An increase in Taylor number tends to homogenise the mechanical treatment in the SSHE.

The development of shear heterogeneities observed in bowls is mainly influenced by the flow behaviour. The appearance of Taylor vortices in bowls, in particular, despite a deformed shape, considerably changes shear conditions and mixing; the thermal treatment must be improved. In the scraped part of the exchanger, flow visualisation revealed that shear heterogeneities can be

explained by the large difference in viscosity in the product in the radial direction at low Taylor number, which induces complex spiral laminar flow.

References

1. E. Dumont, F. Fayolle and J. Legrand, *J. Food Eng.* **45** (2000) 195.
2. A.M. Trommelen, W.J. Beek and H.C. Van De Westelaken, *Chem. Eng. Sci.* **26** (1971) 1987.
3. J.F. Maingonnat and G. Corrieu, *Entropie* **111** (1983) 37.
4. M. Härröd, *J. Food Proc. Eng.* **9** (1986) 1.
5. H. Abichandani, S.C. Sarma and D.R. Heldman, *J. Food Proc. Eng.* **9** (1987) 121.
6. J.C. Leuliet, J.F. Maingonnat and G. Corrieu, *J. Food Eng.* **5** (1986) 153.
7. J.F. Maingonnat, J.C. Leuliet and T. Benezech, *Revue Générale de Thermique* **306–307** (1987) 381.
8. M. Naimi, *Ph.D. thesis*, ENSEM – LEMTA, INP Lorraine (1989).
9. M. Härröd, *J. Food Proc. Eng.* **13** (1990) 59.
10. E. Dumont, D. Della Valle, F. Fayolle and J. Legrand, *J. Food Proc. Eng.* **23** (2000) 207.
11. R. De Goede and E.J. De Jong, *Chem. Eng. Sci.* **48** (1993) 1393.
12. M. Baccar and M.S. Abid, *Récents Progrès en Génie des Procédés* **11** (1997) 219.
13. M. Stranzinger, K. Feigl and E. Windhab, *Chem. Eng. Sci.* **56** (2001) 3347.
14. J. Mabit, C. Loisel, F. Fayolle and J. Legrand, *J. Food Eng.* **57** (2003) 165.
15. J. Mabit, F. Fayolle and J. Legrand, *Chem. Eng. Sci.* **58** (2003) 4667.
16. E. Dumont, F. Fayolle and J. Legrand, *Récents Progrès en Génie des Procédés* **13** (1999) 401.
17. L.P. Reiss and T.J. Hanratty, *AIChE J.* **8** (1963) 154.
18. V. Sobolik, J. Tihon, O. Wein and K. Wichterle, *J. Appl. Electrochem.* **28** (1998) 329.
19. J. Legrand, E. Dumont, J. Comiti and F. Fayolle, *Electrochim. Acta* **45** (2000) 1791.
20. E. Dumont, F. Fayolle and J. Legrand, *Int. J. Heat Mass Trans.* **45** (2002) 679.
21. C. Nouar, *Ph.D. thesis*, ENSEM – LEMTA, INP Lorraine (1986).
22. V.M. Balasubramaniam and S.K. Sastry, *J. Food Proc. Eng.* **19** (1996) 75.
23. S. Wronski and M.S. Jastrzebski, *Int. J. Heat Mass Trans.* **33** (1990) 1.
24. W. Wang, J.H. Walton and K.L. McCarthy, *J. Food Proc. Eng.* **23** (2000) 403.